Design and Analysis of a Linear Induction Motor for a Prototype HTS Maglev Transportation System

Youguang Guo, Wei Xu, Jianguo Zhu, Haiyan Lu, Yi Wang
Faculty of Engineering and Information Technology
University of Technology Sydney
Sydney, Australia
youguang@eng.uts.edu.au, joe@eng.uts.eud.au

Jianxun Jin
Center of Applied Superconductivity and Electrical Engineering
University of Electronic Science and Technology of China
Chengdu, China
jxjin@uestc.edu.cn

***Abstract*— This paper investigates the design and analysis of a linear induction motor (LIM) drive for a prototype transportation system, which is levitated by the interaction force between high temperature superconducting (HTS) bulks placed on the ground and permanent magnets (PMs) mounted on the bottom of the vehicle, while the driving force is provided by a linear induction motor system on the side of the prototype vehicle. An equivalent electrical circuit is applied to predict the motor characteristics and the computation results show that the proposed LIM drive system is appropriate for driving the HTS maglev transportation prototype.**

Keywords-linear induction motor; high temperature superconducting (HTS) maglev transportation system; equivalent electrical circuit.

I. INTRODUCTION

High temperature superconducting (HTS) maglev transportation systems have attracted strong interest of research and development due to their attractive property of high levitation force density with passive and self-stabilizing feature [1]-[2]. For investigating the application of this technique, the authors of this paper have developed a prototype HTS maglev transportation vehicle and a linear permanent magnet (PM) synchronous motor drive, which have been successfully tested in laboratory [3]-[4]. In this paper, we will further develop a linear induction motor (LIM) for driving the HTS maglev vehicle prototype.

For the LIM drive, one can choose a long and active primary track or a short and passive primary track. For long transportation application, the coils and iron core have to be mounted all the way and this would be costly. Furthermore, the supply for the whole primary windings would waste much energy while only the coils facing to the vehicle produce effective force. Segment energizing technique may be used but this causes additional complexity [5]. However, the long primary track can avoid the drawback of sliding contact for supplying the coils and it also has the advantage of light weight vehicle due to the lack of coils and iron core in the vehicle. Therefore, the LIM prototype with short and passive secondary aluminum track to be presented in this paper can be suitable for the launcher system in an airplane carrier, where the primary windings and the HTS bulks are not so long and costly. This paper presents the design and performance analysis of a linear induction motor drive, including the major dimensions and parameters of the motor, drive scheme, parameter computation and performance prediction.

II. PROTOTYPE MAGLEV VEHICLE WITH LIM DRIVE

Fig. 1 illustrates the schematic diagram of the prototype HTS maglev vehicle driven by LIM. The levitation force as well as the guidance force is produced by the interaction between the permanent magnets (PMs) mounted on the bottom of the vehicle and the HTS bulks placed on the ground, while the driving force is generated by two LIMs, one in each side. The LIM consists of a stationary side (copper coils placed in the slots of side steel track) and a movable side (aluminum plate on the vehicle side).

Fig. 2 shows the side view of the stationary part of the LIM formed by stacking a number of modular laminated steel cores along the moving direction. Each modular core consists of a concentrated coil and the coils are connected into three-phase windings and supplied by a varying voltage varying frequency inverter. The slot has a depth of 75 mm and a width of 25 mm. The width of middle tooth is 50 mm, the width of side tooth is 25 mm, the height of yoke is 25 mm, and the transversal length of the modular core is 100 mm.

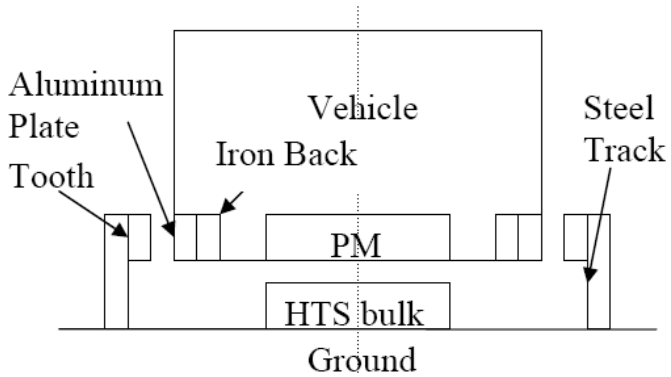

Figure 1. Schematic diagram of an HTS maglev vehicle with LIM drive

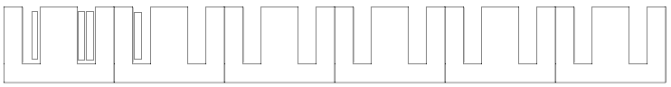

Figure 2. Side view of the stationary part of LIM

III. EQUIVALENT ELECTRICAL CIRCUIT OF LIM

The performance of the LIM can be analyzed by an equivalent electrical circuit as shown in Fig. 3 , where U_1 is the applied phase voltage, r_1 the primary resistance, x_1 the primary leakage reactance, x'_2 the secondary leakage reactance, and r'_2 the secondary resistance referred to the primary side. Compared to the rotary induction motor, the LIM has ends in both longitudinal and transversal directions. To consider the end effects, four correction factors, i.e. the longitudinal end effect factors, $K_r(s)$ and $K_x(s)$, and the transversal end effect factors, $C_r(s)$ and $C_x(s)$, are introduced in the equivalent circuit in Fig. 3. These factors are closely related to the structural dimensions, material properties and velocity of the motor. They can be obtained by numerical magnetic field analysis and/or empirical analytical formulae [6]-[7].

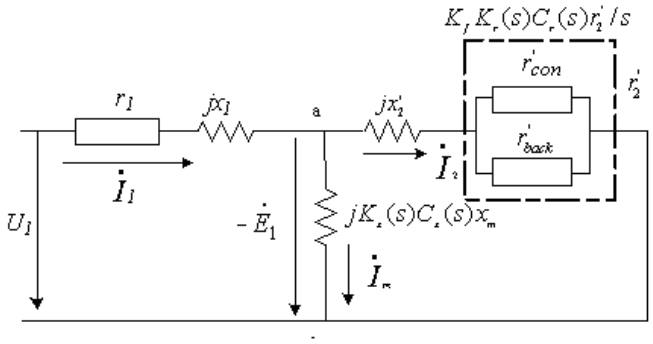

Figure 3. T equivalent electrical circuit of LIM

To achieve the optimal drive performance, the excitation current frequency and motor slip should change according to the vehicle speed. The depth of magnetic field into the secondary aluminum sheet is calculated by

$$\delta = \sqrt{\frac{2}{\omega \mu \delta}} \tag{1}$$

When the secondary current frequency is 25 Hz, the penetration depth of magnetic flux into the aluminum sheet is calculated as 18.3 mm. Therefore, in most operational conditions, the magnetic flux can reach the back iron and the secondary resistance should include both the conduction sheet resistance and the back iron resistance, i.e. r_{con} and r_{back}.

The skin-effect factor K_f is obtained by

$$K_f = \frac{1 + B_1^2 sh^2(2Kg_e)}{A_1[1 + B_1^2 sh^2(2Kd)]} \tag{2}$$

where $K=\pi/\tau$, τ is the primary pole pitch, d is the thickness of the secondary conduction sheet, g_e is the equivalent air gap length, and A_1 and B_1 are coefficients which are the functions of the slip and motor structure as

$$g_e = K_c K_u g \tag{3}$$

$$A_1 = ch^2(Kg_e) + [\frac{K\rho_{Al} sh(Kg_e)}{s\omega\mu_0 d}]^2 \tag{4}$$

$$B_1 = \frac{s\omega\mu_0 d}{2K\rho_{Al}}\left(1 + \frac{K\rho_s}{s\omega\mu_0 d}\right)^2 \tag{5}$$

where g is the air gap length, K_c the Carter factor, K_u the magnetic saturation factor, ρ_{Al} the electrical conductivity of the secondary aluminum sheet, s the slip, ω the angular frequency of induced secondary current, and μ_0 the magnetic permeability of air.

The primary winding resistance can be calculated by

$$r_1 = 2\rho_{cu} l_1 W_1 / S_{cu} \tag{6}$$

where ρ_{cu} is the resistivity of copper, l_1 the length of half coil, W_1 the number of turns of phase winding in series, and S_{cu} the cross-sectional area of the copper wire.

The primary leakage reactance can be calculated by

$$x_1 = 0.158 f_1 W_1^2 \frac{a_1}{q}\left(\frac{\lambda_s}{P} + \frac{\lambda_t + \lambda_e + \lambda_d}{P_e}\right) \tag{7}$$

where f_1 is the primary current frequency, a_1 the width of primary lamination, P the number of pole pairs, P_e the number of equivalent pole pairs, λ_s the slot magnetic leakage permeance, λ_t the tooth leakage permeance, λ_e the end leakage permeance, and λ_d the harmonic leakage permeance,

The secondary winding resistance consists of two parts: the aluminum sheet resistance and the back iron resistance in parallel as shown in Fig. 3. The aluminum sheet resistance can be calculated by

$$r_{con} = \frac{2m_1\rho_{Al} W_1^2 k_{w1}^2 a_1}{P_e d\tau} \tag{8}$$

where m_1=3 is the number of phases of primary winding, k_{w1} the primary winding factor, and ρ_{Al} the resistivity of aluminum sheet.

The back iron resistance is calculated by

$$r_{back} = \frac{2m_1\rho_{Fe} W_1^2 k_{w1}^2 a_1}{P_e d_{Fe}\tau} \tag{9}$$

where ρ_{Fe} is the resistivity and d_{Fe} is the thickness of the back iron.

Therefore, the secondary resistance is

$$r_2 = \frac{r_{con} r_{back}}{r_{con} + r_{back}} \tag{10}$$

The secondary leakage reactance is calculated by

$$x_2 = k_f \frac{r_2}{s} B_1 sh(2Kd) \tag{11}$$

The exciting reactance is calculated by

$$x_m = \frac{2m_1\mu_o W_1^2 k_{w1}^2 a_1 v_s}{\pi g_e P_e} \quad (12)$$

where v_s is the synchronous velocity of primary magnetic field.

IV. Performance Analysis

The major dimensions and parameters of the proposed LIM include the rated primary voltage of 380 V, rated primary current of 37 A, rated apparent power of 24 kVA, rated output power of 8.5 kW, rated driving force of 780 N, vehicle length of 1.65 m, and main air gap length of 10 mm.

Based on the equivalent circuit, the major characteristics of LIM can be obtained. For example, the curve of thrust force versus velocity is shown in Fig. 4. The thrust force is actually determined by the load, i.e. the wind and friction resistances and acceleration. Below the base velocity, the LIM adopts the constant force control so that the thrust force is almost constant. Above the base velocity, the LIM adopts the constant power control so that the output power is almost constant; the phase voltage has reached its maximum value but the reactance continues to increase, so the phase current should be controlled to decrease as well as the thrust.

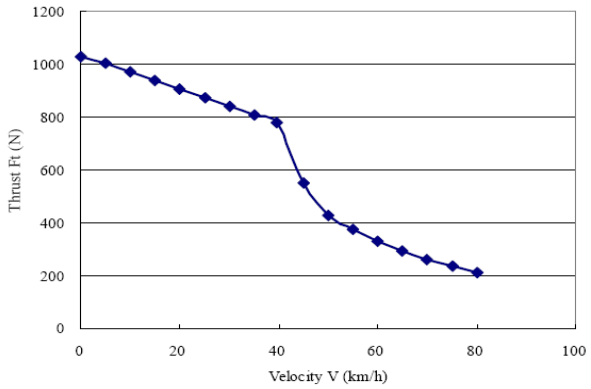

Figure 4. Curve of thrust force versus velocity

Fig. 5 illustrates the relation between the phase voltage and vehicle velocity. It can be seen that under 40 km/h, the vehicle velocity is controlled by the applied voltage under the constant torque control mode. When the voltage reaches the rated value, the vehicle velocity is adjusted by applying the flux-weakening technique under the constant power control mode. The corresponding phase current is given in Fig. 6.

Fig. 7 shows the LIM drive power factor, efficiency, and product of power factor and efficiency. Fig. 8 plots the drive capacity, input power and output power with respect to vehicle velocity.

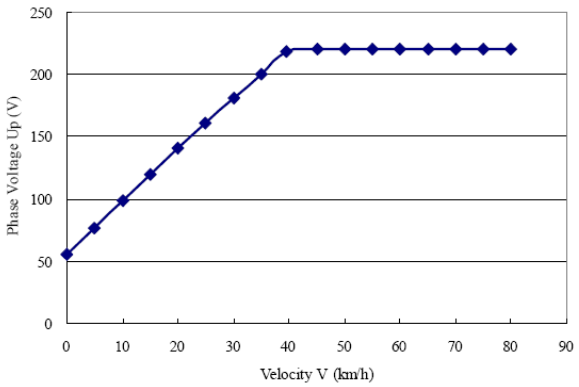

Figure 5. Phase voltage against veclocity

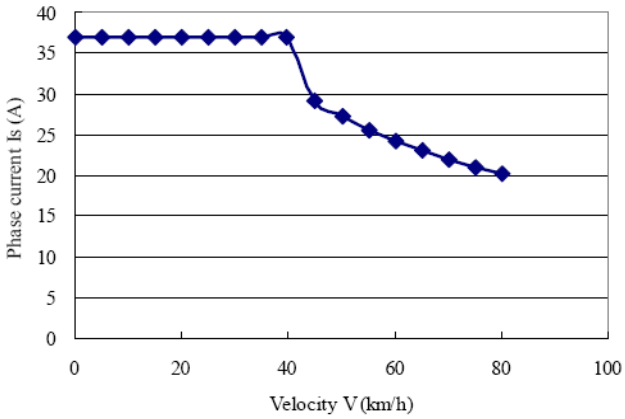

Figure 6. Curve of phase current versus velocity

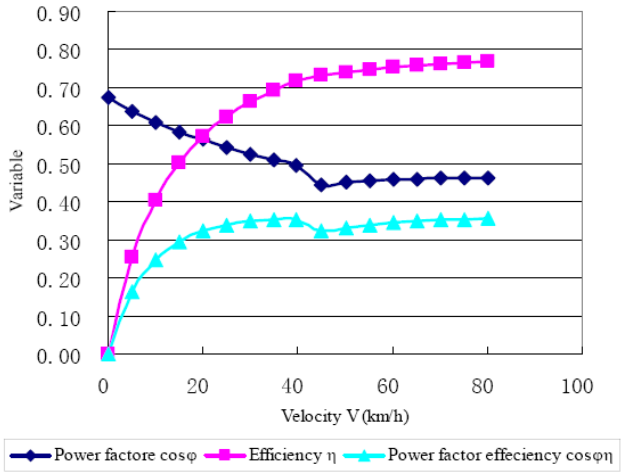

Figure 7. Power factor, efficiency, and power factor efficiency vesus veclocity

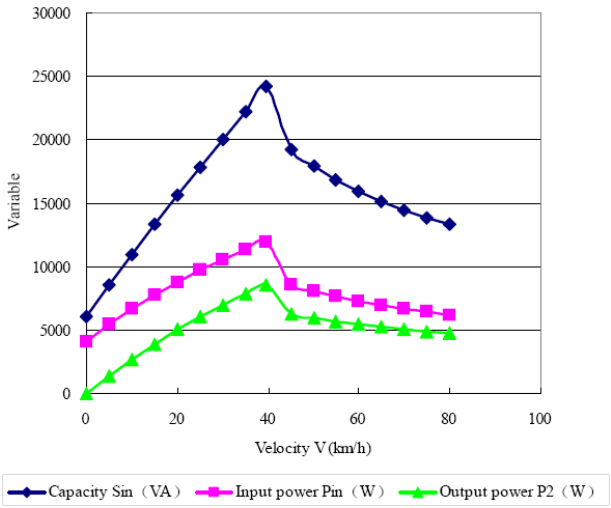

Figure 8. LIM drive capacity, input power and output power versus velocity

V. CONCLUSION

This paper presents the design of a linear induction motor drive for a HTS maglev vehicle prototype. The major characteristics of the linear motor are predicted by an improved equivalent electrical circuit, which takes into account the end effects, back-iron saturation and skin effect. The calculated performance, including the thrust force, phase voltage, phase current, power factor, efficiency and power against velocity, shows that the designed motor would be appropriate.

REFERENCES

[1] T. Takao, A. Niiro, S. Suzuki, *et al.*, "Experimental and numerical analysis of lift force in magnetic levitation system," *IEEE Trans. Appl. Supercond.*, vol. 15, no. 2, pp. 2281-2284, 2005.

[2] J. Bankuti, I. Vajda, L. Mohacsi, *et al.*, "Design and construction of a small-scale model of a high-temperature superconducting magnetically levitated vehicle," *IEEE Trans. Magn.*, vol. 32, no. 4, pp. 2288-2291, 1996.

[3] J.X. Jin, Y.G. Guo, J.X. Chen, L.H Zheng, and J.G. Zhu, "HTS levitation and transportation with linear motion control," in *Proc. 26th Chinese Control Conf.*, Zhangjiajie, China, July 2007, pp. 3325-3329.

[4] Y.G. Guo, J.X. Jin, L.H. Zheng, J.G. Zhu, and H.Y. Lu, "A permanent magnet linear synchronous motor drive for HTS maglev transportation system,", *HTS Special Issue of Journal of Electronic Science and Technology of China*, vol. 6, no. 2, pp. 125-129, June 2008.

[5] G.W. Mclean, "Review of recent progress of linear motors," *IEE Proceedings – Part B*, vol. 135, no. 6, pp. 380-416, 1988.

[6] W. Xu, G. Sun, and Y. Li, "Research on tractive charateistics of the single linear induction motor," in *Proc. Int. Conf. on Industrial Technology*, 2006, pp. 510-516.

[7] W. Xu, J. G. Zhu, L. Tan, Y. G. Guo, S. H. Wang, and Y. Wang, "Optimal design of a linear induction motor applied in transportation," in *Proc. Int. Conf. on Industrial Technology*, Gippsland, Australia, Feb. 2009, pp. 790-794.